Transport Anomalies Emerging from Strong Correlation in Ionic Liquid Electrolytes

Nicola Molinari,[*,†] Jonathan P Mailoa,[‡] Nathan Craig,[¶] Jake Christensen,[¶] and Boris Kozinsky[*,†,‡]

†*John A. Paulson School of Engineering and Applied Sciences, Harvard University, Cambridge, MA 02138, USA*

‡*Robert Bosch LLC, Research and Technology Center, Cambridge, MA 02142, USA*

¶*Robert Bosch LLC, Research and Technology Center, Sunnyvale, CA 94085, USA*

E-mail: nmolinari@seas.harvard.edu; bkoz@seas.harvard.edu

Graphical TOC entry

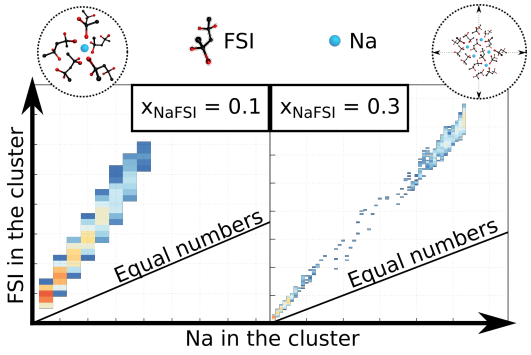

Abstract

Strong ionic interactions in concentrated ionic liquids is shown to result in significant correlations and deviations from ideal solution behavior. We use rigorous concentrated solution theory coupled with molecular dynamics simulations to compute and explain the unusual dependence of transport properties on cation concentration in the Na^+-$Pyr_{13}{}^+$-FSI^- ionic liquid electrolyte. When accounting for intra- and inter-species correlation, beyond the commonly used uncorrelated Nernst-Einstein equation, an anomalously low and even negative transference number emerges for x_{NaFSI} lower than 0.2. With increasing concentration the transference number monotonically increases, approaching unity, while the total conductivity decreases as the system transitions to a state resembling a single-ion solid-state electrolyte. The degree of spatial ionic association is explored further by employing unsupervised single-linkage clustering algorithm. We emphasize that strong ion-ion coupling in the electrolyte significantly impacts the trade-off between key electrolyte transport properties, and consequently governs the power density of the battery.

Introduction

Rapidly developing technologies in transportation and stationary energy storage demand rechargeable batteries that can reliably deliver more energy and power at lower cost. Mobile applications are adopting Li-ion batteries due to their high volumetric and gravimetric energy density, but stationary storage applications are more focused on the cost aspect, driving research efforts in the Na-ion technology.[1–3] While significant research efforts are devoted to higher-capacity cathode materials, it is realized that properties of electrolytes primarily control the power and safety of battery cells,[4–7] particularly important aspects for stationary grid-energy storage solutions.

Electrolyte solutions typically contain high concentrations of an alkaline-ion salt in order to optimize transport properties, which determine charge and discharge rate capabilities of

the cell. Specifically, what should be maximized is not the total ionic conductivity, which has contributions from all charged and mobile species in the system, but the fraction of conductivity due to the cation of interest (for instance Na^+), which is measured by the product of the total conductivity and the transference number t^+_{Na}.[3] Surprisingly, despite the ionic nature as well as the high alkaline-ion salt concentrations often used, the studies aimed at developing a fundamental understanding of transport properties systematically adopt a dilute limit approach based on the Nernst-Einstein relation,[8,9] where inter- and intra-species correlations are ignored.[10–14] In computer simulations, it is often assumed that the overall effect of correlation on the absolute values of conductivity is small at low enough salt concentrations. However, there is no a priori justification for making this approximation in strongly interacting highly concentrated solutions. Additionally, as we demonstrate, transport properties that are of key importance for practical applications, such as the transference number, can exhibit fundamentally different behaviors when correlation is taken into account. A negative transference number has been recently measured experimentally in both polymer- and ionic liquid-based electrolytes,[15,16] yet the commonly-adopted Nernst-Einstein approach for uncorrelated diffusion cannot yield a negative transference number.

In this work we showcase the importance of including ion-ion correlations by combining molecular dynamics simulations with fully-correlated concentrated-solution theory. To illustrate the importance of ionic correlations, we examine transport characteristics of concentrated ionic liquid electrolytes. Room temperature ionic liquids (or RTILs) exhibit properties such as low volatility, low flammability, and higher chemical and thermal stability as opposed to standard organic solvents, which make them attractive for technological applications as electrolytes.[17–21] RTILs composed of Na^+ / bis(fluorosulfonyl)imide (or Na^+FSI^-) in N-propyl-N-methylpyrrolidinium / bis(fluorosulfonyl)imide (or $Pyr_{13}{}^+FSI^-$) have been experimentally investigated up to remarkably high Na^+FSI^- molar fractions, and they exhibit stable cycling at high currents as well as promising transport properties .[12,22,23] Especially interesting are the trends of increasing t^+_{Na} with increasing molar fractions of Na^+FSI^- in

$Pyr_{13}{}^{+}FSI^{-}$, while simultaneously the overall ionic conductivity is decreasing.[12,22,24] As mentioned above, optimization of electrolyte transport properties needs to quantitatively consider the trade-off between these two trends. A deeper understanding of these findings and the underlying physical transport mechanisms is needed to enable quantitative design and optimization of this and other electrolyte systems.

As speculations around the aforementioned experimental observations suggest cation-anion aggregation and changes in the cation coordination environment, computer simulations provide a powerful framework to gain fundamental understanding and complement the experimental observations. Molecular dynamics (or MD) simulations can be leveraged to obtain atomistic-level insights into the coordination, mobility, and aggregation between different species, which are nearly inaccessible by experimental studies. It should also be noted that it is rather difficult to reliably measure transference numbers experimentally,[25] and MD simulations provide a key complementary investigation tool. Previous MD studies of this electrolyte highlighted the importance of the relationship between sodium dynamics, and the Na^{+}-N_{FSI^-} and N_{FSI^-}-N_{FSI^-} radial distribution functions (RDF).[11] Using RDFs at different $Na^{+}FSI^{-}$ concentrations, they hinted at rearrangements of the FSI^{-} anion, possibly due to the formation of agglomerates, previously postulated to explain the low measured values of t^{+}_{Na} at low x_{NaFSI}.[12] Despite the strong evidence of significant ionic interactions, computational analysis of this and similar ionic liquid systems have only been studied using ideal solution theory and uncorrelated transport analysis, resulting in limited accuracy due to uncontrolled approximations. Moreover, while $Na^{+}FSI^{-}$ agglomerates are conjectured to explain the observed trends in transport properties of this system, no direct characterization has been proposed; therefore, there is a missing direct link between correlated ion motion and $Na^{+}FSI^{-}$ cluster population. Such deeper understanding would not only uncover new insights for this system as well as help ingraining current belief, but also serve as case study for the importance of ion correlation in RTIL-based super-concentrated electrolytes.

Our approach, based on a rigorous combination of molecular dynamics with concen-

trated solution theory, accounts for intra- and inter-species correlation and is able to recover and explain experimentally observed trends in t^+_{Na}. Most notably, a negative t^+_{Na} is found for x_{NaFSI} lower than 0.2. Above this concentration t^+_{Na} becomes positive and steadily increases to values closely matching experimental findings measured with the Bruce and Vincent method (that assumes ideal solution behavior).[26,27] Also, thanks to the atomistic resolution of the MD approach, we are able to link experimental findings to the formation of Na^+FSI^- aggregates, which were previously only postulated and that we are able to directly quantify in our work.

Methods

Structures Generation

To create a low-density non-overlapping initial structure, we place Na^+, $Pyr_{13}{}^+$ (Figure 1a), and FSI^- (Figure 1b) randomly on the vertices of a three-dimensional cubic grid .[28] The

(a) $Pyr_{13}{}^+$ (b) FSI^-

Figure 1: Molecular structure of the $Pyr_{13}{}^+$, (a), and FSI^-, (b), molecules.

equilibration routine (described later) is used to bring the systems to equilibrium density, as there are no entanglement effects at the length-scales that characterize the (small) molecules under investigation. We study the range from $x_{NaFSI} = 0.0$ to $x_{NaFSI} = 1.0$ with increments of $x_{NaFSI} = 0.1$. Note that $x_{NaFSI} = 0.0$ corresponds to a pure $Pyr_{13}{}^+FSI^-$ ionic liquid system, while $x_{NaFSI} = 1.0$ is a pure Na^+FSI^- salt system. The total number of atoms as well as the number of Na^+, $Pyr_{13}{}^+$, and FSI^- molecules for all x_{NaFSI} in our simulations is reported in the Supplementary Information, Section 1. To compute ensemble averages and minimize the impact of the structure generation, four independently-generated structures are used

for each x_{NaFSI}. The uncertainties for all the reported quantities are computed as standard deviations among the ensemble of four structures at a given x_{NaFSI}, unless otherwise stated.

Molecular Dynamics Details

All molecular dynamics (MD) simulations have periodic boundary conditions and are performed using the freely-available LAMMPS code.[29] We adopt the Optimized Potentials for Liquid Simulations (OPLS) force-field from Schrodinger Inc.[30] to model the atomic interactions. As commonly done in the ionic liquid literature to mimic the average charge screening due to polarisation, and charge transfer effects, for instance,[31–33] in this work the point charges assigned to every atomic species are rescaled. The cost-effective charge-rescaling is generally adopted to avoid polarisable models, such as self-consistent inducible dipoles[34] or Drude oscillators,[35] since their positive gains are counterbalanced by a significant increase in computational cost. In particular, we find that charges reduced to 75 % of their original values well reproduce experimental mass density data, as we report in the first part of the result section. The equation of motions are evolved using a velocity-Verlet integrator with a timestep of $\delta t = 1.5\,\mathrm{fs}$. Temperature and pressure of the simulations are enforced using a Nosé-Hoover barostat ($1000\,\delta$t coupling) and thermostat ($100\,\delta$t coupling), respectively.[36–38] Once generated, the structures are equilibrated in order to overcome local energy barriers in search of lower energy minima. The equilibration routine is a multi-stage simulation including energy minimizations, compression/decompression, and annealing stages broadly based on previous works.[39,40] Specific details of the equilibration stages can be found in the supplementary information, Section 2. The production runs for the computation of the transport properties are performed after the equilibration. The Na^+FSI^--$Pyr_{13}{}^+FSI^-$systems are evolved for 75 ns in order to compute the diffusion properties, namely conductivity, and sodium transference number. These systems are well within the diffusive regime at this time-scales; an example plot of the mean-squared displacement (MSD) for $x_{NaFSI} = 0.1$ is provided in the supplementary information, Section 3.

Uncorrelated Analysis

The mean-squared displacement (or MSD, Eq. 1) is the most widely adopted approach to analyze trajectory data to extract transport properties.

$$\mathrm{MSD}_i = \langle r^2(t) \rangle_i = \langle |\vec{r}(t) - \vec{r}(0)|^2 \rangle_i. \tag{1}$$

$\langle \cdot \rangle_i$ indicates the ensemble average over species i. Using the Einstein relation,[8,9] the diffusion constant for particle species i, D_i, can be calculated as the slope of the MSD, Eq. 2.

$$D_i = \frac{1}{6} \lim_{t \to \infty} \frac{\partial \ \mathrm{MSD}_i(t)}{\partial \ t} \tag{2}$$

D_i is often addressed as tracer diffusion constant, as it can be experimentally measured with isotopic tracer particles, or equivalently with pulsed field gradient NMR. Once the diffusion constant of all the species is computed, the total conductivity of the system can be estimated using the Nernst-Einstein relation,[8,9] Eq. 3.

$$\kappa_{\mathrm{NE}} = \frac{e^2}{V k_B T} \sum_i n_i q_i^2 D_i. \tag{3}$$

Where V is the total volume of the simulation, e the elementary charge, T the temperature, k_B the Boltzmann constant, n_i the number of atoms/molecules of the species i, q_i their numeric charge and D_i their tracer diffusion constant. Similarly, the transference number of species i can be defined in terms of the tracer diffusion constants as in Eq. 4.[41]

$$t^i_{\mathrm{NE}} = \frac{q_i^2 n_i D_i}{\sum_i q_i^2 n_i D_j} \tag{4}$$

The key advantage of the MSD method lies in its significantly quicker convergence as a function of MD trajectory time, resulting from dropping the cross-correlation terms between particles, effectively assuming all moving objects are independent. In other words, both the

inter- and intra-species correlations are ignored.

Correlation analysis

While it may be reasonable for some systems in dilute regimes, the no-correlation assumption of the MSD approach can hide important physical insights. For ionic liquid systems it is easy to imagine how an approach accounting for the correlation between ions is needed. In this work we compute transport properties of correlated systems using equilibrium MD simulations, adopting the theory of transport in multicomponent concentrated solutions by Wheeler and Newman,[42] and compare to the uncorrelated approximation. In this framework, we use the position correlation function (or PCF) to compute conductivity and t^{+}_{Na} from the symmetric mass-transport matrix L. The coefficients L_{ab} are obtained from the slope of the dot product between the position vectors of the centers of mass of species a, R_a, and b, R_b, over time; see Eq. 5 and Eq. 6.

$$\mathrm{PCF}_{ab}(\tau) = \frac{V}{6k_B T}\left\langle \left[\vec{R}_a(\tau) - \vec{R}_a(0)\right] \cdot \left[\vec{R}_b(\tau) - \vec{R}_b(0)\right] \right\rangle \tag{5}$$

$$L_{ab} = \lim_{\tau\to\infty} \frac{\partial\ \mathrm{PCF}_{ab}(\tau)}{\partial\ \tau} \tag{6}$$

To better understand the meaning of the L_{ab} coefficients, a couple of possible scenarios are described in the Supplementary Information, Section 3. Additionally, in the same Section an example plot showing the L_{ab} values versus time in the case of $x_{NaFSI} = 0.1$ is presented.

Once the L matrix is obtained, the conductivity is calculated as shown in Eq. 7.[42,43]

$$\kappa_C = \sum_{ab} \theta_a \theta_b L_{ab}. \tag{7}$$

$\theta_j = F q_j c_j$, F is the Faraday's constant, and q_j and c_j are the charge number and concentration of species j, respectively. The ratio $\lambda = \kappa_C/\kappa_{NE}$ is often used to quantify the degree of correlation of a system. When $\lambda = 1$, correlation does not contribute towards the total

conductivity, if $\lambda < 1$ or $\lambda > 1$, correlation contributes negatively/positively to the total conductivity. Importantly, the L_{ab} elements can also be used to calculate the correlated transference number of species a as in Eq. 8.[43]

$$t_{\mathrm{C}}^{a} = \frac{\sum_{b} \theta_a \theta_b L_{ab}}{\sum_{bc} \theta_b \theta_c L_{bc}} \tag{8}$$

Our choice of reference position is the center of mass of the system as there is no species that could be treated as "solvent".

Results and Discussion

Density and Radial Distribution Function

To validate the force-field and especially the 75 % charge rescaling applied to the system, we compute the mass density at different x_{NaFSI} and temperatures, and compare the results with experimental values. Here a brief summary of the findings is presented, and a full discussion can be found in the Supplementary Information, Section 5. Figure 2 summarizes the computed (empty shapes) and experimental[22] (full shapes) densities for three x_{NaFSI} at different temperatures. We find excellent agreement between the density values from experiment and molecular dynamics, as the general trends are reproduced, and the absolute values are closely matched. It is worth highlighting that we investigated different point charge rescaling values and, remarkably, the rescaling was found not to depend on x_{NaFSI}. The general observed trend follows intuition: the smaller the charge rescaling factor, the greater the over-estimation of the density across all x_{NaFSI} and temperature. This can be observed in Section 4 of the Supplementary Information, where we report two density plots equivalent to that of Figure 2, but obtained for charge rescalings of 80 % and 90 %.

We also calculate the Na^+ radial distribution function (RDF) with the oxygen atoms in the system (the only source of oxygen atoms is the FSI^- anion, see Figure 1), details in

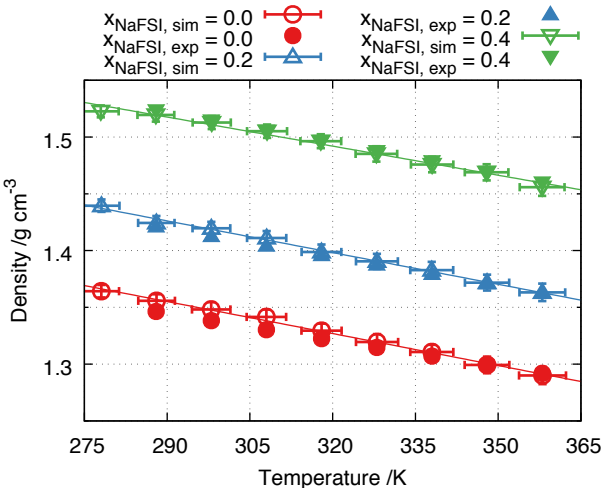

Figure 2: Density values as a function of temperature for three different x_{NaFSI} as computed in this work (sim, empty shapes) and from experiment (exp,[22] full shapes) to validate the charge rescaling and force-field used. Whilst always present, some of the uncertainties are small and cannot be appreciated at the scale of the plot.

Section 6 of the Supplementary Information. Figure 3 summarizes the RDFs for two different x_{NaFSI} from this work (red curves), and from other MD simulations from the literature using different force-fields and adopting different charge rescaling factors[11] (blue and green curves). For the RDFs from this work, the uncertainty is plotted as shaded area around the mean (solid red line), however, it is not appreciable on the scale of the plot. The paucity of experimental Na^+ RDFs for this systems prevented us from comparing our results directly to experiment. For both $x_{NaFSI} = 0.1$ and $x_{NaFSI} = 0.9$ (corresponding to a dilute and highly concentrated Na^+FSI^- in $Pyr_{13}{}^+FSI^-$ solutions, respectively), the Na^+ RDFs from this work well reproduce MD results from the literature.[11] The intensity of our peaks (with a point charge rescaling factor of 75 %) lies in-between the one obtained from other MD works with a 100 % and 67 % charge rescaling factors. Most importantly, the overall structural properties are not altered by the charge rescaling: the positions of both the peaks and the minima are in good agreement. The first minimum of the Na^+-O RDF, corresponding to the first coordination cage, is approximately independent of the x_{NaFSI}, and it is found to be at approximately 3.65 Å. Finally, in[31] rescaled atomic charges for the OPLS force-field are thoroughly tested and shown to reproduce quite well a wide range of properties as compared

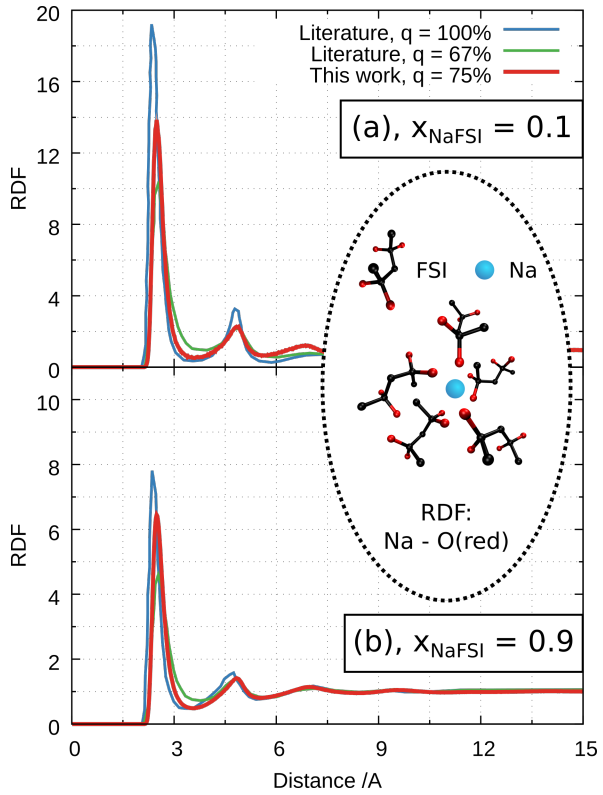

Figure 3: Radial distribution function (RDF) between sodium and oxygen atoms for two different x_{NaFSI} as computed in this work (red curves, 358 K), and other MD literature values with different charge rescaling factors[11] (blue and green curves, 393 K). The uncertainty for the RDFs from this work is displayed as shaded area around the mean, however, it is not appreciable at the scale of the plot.

to experiments as well as ab initio MD simulations. In their work the authors conclude that charge rescaling is a good alternative to the use of expensive polarisable force-fields. We conclude that the structural properties of the Na^+, FSI^-, and $Pyr_{13}{}^+$ systems can be well-captured by the OPLS force-field from Schrodinger Inc.[30] with a point charge rescaling of 75 %, thus we adopt it throughout.

Coordination and Persistence

Previous reports highlighted the role of the oxygen atoms in the Na^+ coordination, reporting a total coordination of 5/6 oxygen atoms within the first coordination cage, i.e., up to the first minima of the Na^+-O RDF, almost independent of x_{NaFSI}.[12] Here we want to study sodium coordination in more details by looking at the actual distribution in oxygen coordi-

nation as a function of x_{NaFSI}, as well as study the persistence of the coordination. With this goal in mind, after the equilibration routine every structure is evolved for a total of 7.5 ns in a constant number of particles, volume (as obtained from the last stage of the equilibration routine, supplementary information Section 2), and temperature (358 K). Throughout the dynamics, snapshots containing the positions of all atoms are saved every $100\,\delta t = 0.15$ ps for post-processing. For a given sodium, we consider an oxygen as "coordinating" if found within a sphere of radius 3.65 Å (corresponding to the position of the first minimum of the Na^+-O RDF, Figure 3) centered on the Na^+ atom. The coordination of all sodium atoms in all snapshots is obtained from the dynamics of the four structures having the same x_{NaFSI}, and then used to determine the distribution of coordination. Additionally, the resulting distribution of coordination is fitted to a Gaussian distribution.

Figure 4(a), and (b) summarize the results for $x_{NaFSI} = 0.1$, and $x_{NaFSI} = 1.0$, respectively (the plots corresponding to the other x_{NaFSI} are presented in the Supplementary Information, Section 7). We first observe that the mean of the distribution of coordination (X_0 in the top right corners) slightly increases by approximately 7 % in the range of x_{NaFSI} investigated. Its value indicates an average coordination from the oxygen atoms between five and six, confirming previous results from the literature obtained by integrating the Na^+-O RDF.[11,12] The trend in the standard deviation of the distribution of coordination (σ in the top right corners) monotonically increases for greater x_{NaFSI}. In particular, from $x_{NaFSI} = 0.1$ to $x_{NaFSI} = 1.0$ it increases by 37 %. This observation is interesting because even though the average coordination does not substantially change, the specific atoms coordinating with Na^+ cations becomes more variegate. This signals some difference in the overall structure of the system at high x_{NaFSI}. Also, it resonates well with previous experimentally observed variations of the anion environment for the Na^+ cation at different x_{NaFSI} using Raman spectroscopic analysis.[44]

While it is important to understand the local environment of the sodium atoms, the dis-

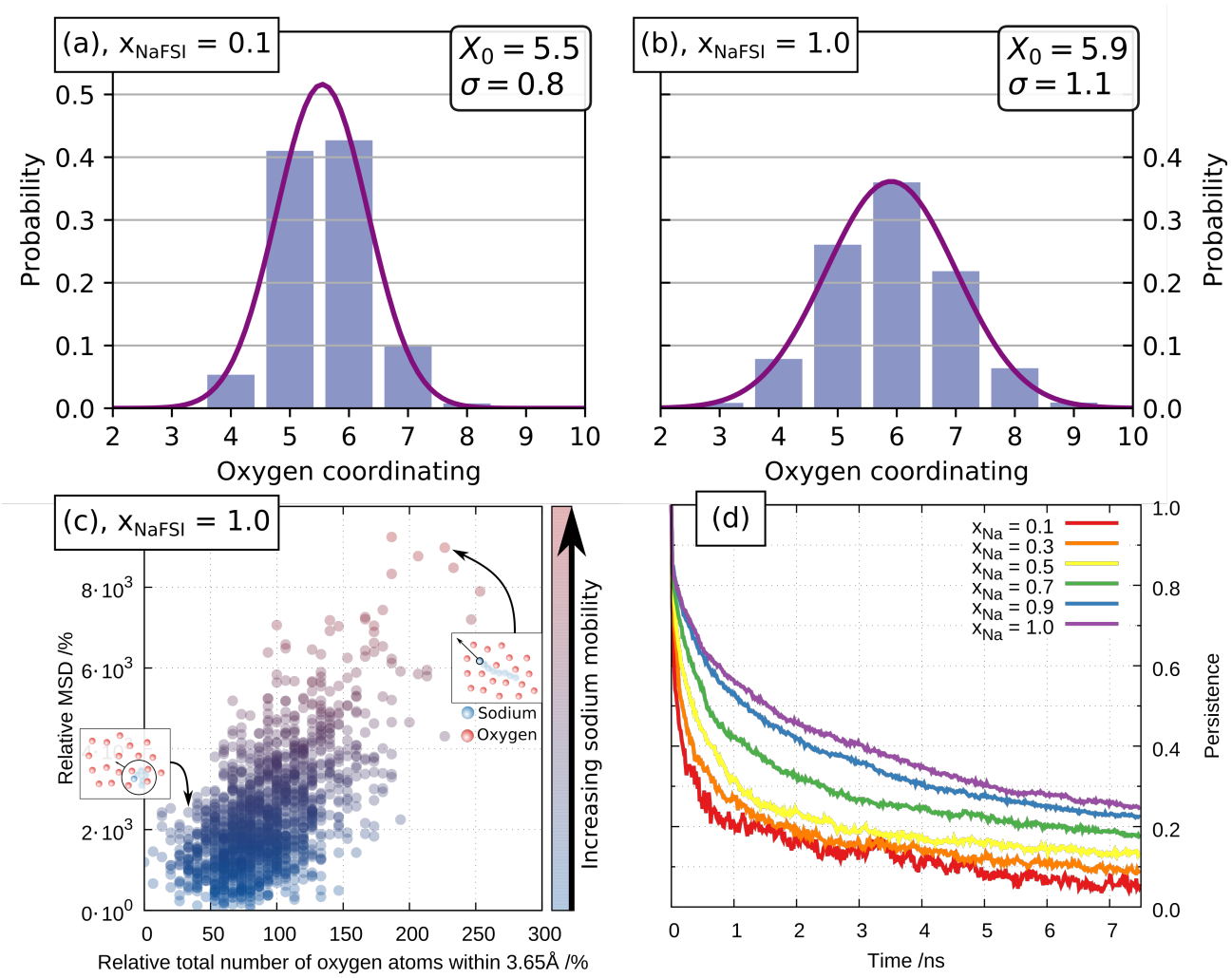

Figure 4: (a), and (b) show the probability of the number of oxygen atoms coordinating a Na^+ for $x_{NaFSI} = 0.1$, and $x_{NaFSI} = 0.2$, respectively. Every histogram is fitted with a Gaussian distribution (dark purple line); X_0 and σ at the top right corner of the (a-b) plots correspond to its mean and standard deviation, respectively. (c) shows the percentage difference in MSD versus the percentage difference in total unique oxygen atoms within 3.65 Å during the whole 7.5 ns simulation. (d) shows the persistence, computed as Eq. 9, of the specific oxygen atoms coordinating a given Na^+ at different x_{NaFSI}.

tribution of coordination does not elucidate the evolution of a specific coordination cage over time. In other words, how stable are the coordination cages over time and how this impact Na^+ mobility? Are the coordinating oxygen remaining the same, meaning the coordinating FSI^- drag/are dragged by Na^+, or does Na^+ constantly jump between different coordination shells? In Figure 4(c) we show the percentage increase in Na^+ MSD as a function of the percentage increase in total number of unique oxygen atoms found coordinating a given

Na^+ during the entire 7.5 ns. Intuitively, sodium experiencing a higher turnover of coordination should be more mobile, and our findings confirm this hypothesis. Also, Figure 4(c) highlights that at $x_{NaFSI} = 1.0$ there exist an uneven distribution of mobility, with only a few Na^+ being highly mobile. To further help answering the above questions, we adopt a modified version of the persistence measure defined in an earlier work.[45] The persistence is defined as the fraction of oxygen atoms coordinating a sodium at time t that remains the same as at time $t' = 0$. In other words, if the persistence is equal to one then the exact same oxygen atoms from $t' = 0$ are coordinating the Na^+ cations at $t'' = t$. If the persistence is equal to zero then a completely different set of oxygen atoms is coordinating the Na^+. More precisely, let G_0^i and G_t^i be the sets containing the indices of the oxygen atoms coordinating sodium i at time 0 and t, respectively. Then the persistence for sodium i at time t, $\mathcal{P}^i(t)$, is defined as:

$$\mathcal{P}^i(t) = \frac{G_0^i \cap G_t^i}{|G_0^i|}. \tag{9}$$

Figure 4(d) shows, for every other x_{NaFSI} starting from $x_{NaFSI} = 0.1$, the persistence value over time, averaged over all the Na^+ and structures with same concentration. The persistence averaged over the ensemble of all sodium, $\langle \mathcal{P}(t) \rangle_{Na}$, starts at one and it decays over time, meaning that, while maintaining the total average coordination as observed previously, the specific oxygen atoms contributing to the coordination change over time. This fact is not surprising per se: Na^+ and FSI^- do not share any actual bond and, especially at the high temperature investigated here, it is to be expected that the specific oxygen atoms coordinating a particular Na^+ cation change over time. We note that this behavior is different in polymer electrolyte systems, where the cation coordination cage can remain unchanged over hundreds of nanoseconds.[40,46] However, the rate of this and its dependence on the salt concentration is surprising for the following reasons. First, for higher x_{NaFSI} the oxygen atoms constituting the coordination cage of a specific Na^+ are substituted at a lower rate, effectively meaning the coordination cage is less stable for lower salt concentrations. As it will be shown later, at 358 K and low x_{NaFSI} both Na^+ and FSI^- are more mobile than

at higher salt concentrations, resulting in less consistent specific coordination. Second, for pure Na^+FSI^- (purple line in Figure 4(d)), after 7.5 ns the coordination of the Na^+ is made, on average, of more than 20 % of the oxygen atoms coordinating it at the beginning of the simulation.

Transport Properties

In order to compute the transport properties of the Na^+FSI^--$Pyr_{13}{}^+FSI^-$ system, the structures are evolved for 75 ns in a constant number of particles, volume (as after the last stage of the equilibration procedure, Section 2 of the supplementary information), and temperature (358 K) ensemble. The MSDs, Eq. 1, and positions of the center of mass of all the species are saved every $10\,k\delta t = 15$ ps for post-processing. The saved information is analyzed using both the Nernst-Einstein approach (which yields transport properties in the limit of no correlation, Eq. 1 to Eq. 4), and the Wheeler-Newman approach [42] (which yields transport properties for correlated systems, Eq. 7 and Eq. 8).

A summary of the transport properties for the Na^+FSI^- in $Pyr_{13}{}^+FSI^-$systems is presented in Figure 5. On the x axes of all plots in Figure 5 there is x_{NaFSI}. Plot (a) shows the conductivity values from experiment [22] (black line), and from our investigation (blue and red referring to the uncorrelated Nernst-Einstein (NE) and correlated (C) approaches, respectively) on the left y axes. On the right y axes of plot (a) we present the ratio $\lambda = \kappa_C/\kappa_{NE}$ (green dots, also known as Haven ratio); the uncertainty on λ is calculated using the error propagation.

Looking at the computed conductivity values (blue and red curves in Figure 5(a)) they are consistently underestimating the experimental values (black curve) by approximately a factor of two. A more aggressive charge rescaling, i.e., lower charges than 75 % of the nominal unit values would increase the diffusivity of all species, yielding a higher total conductiv-

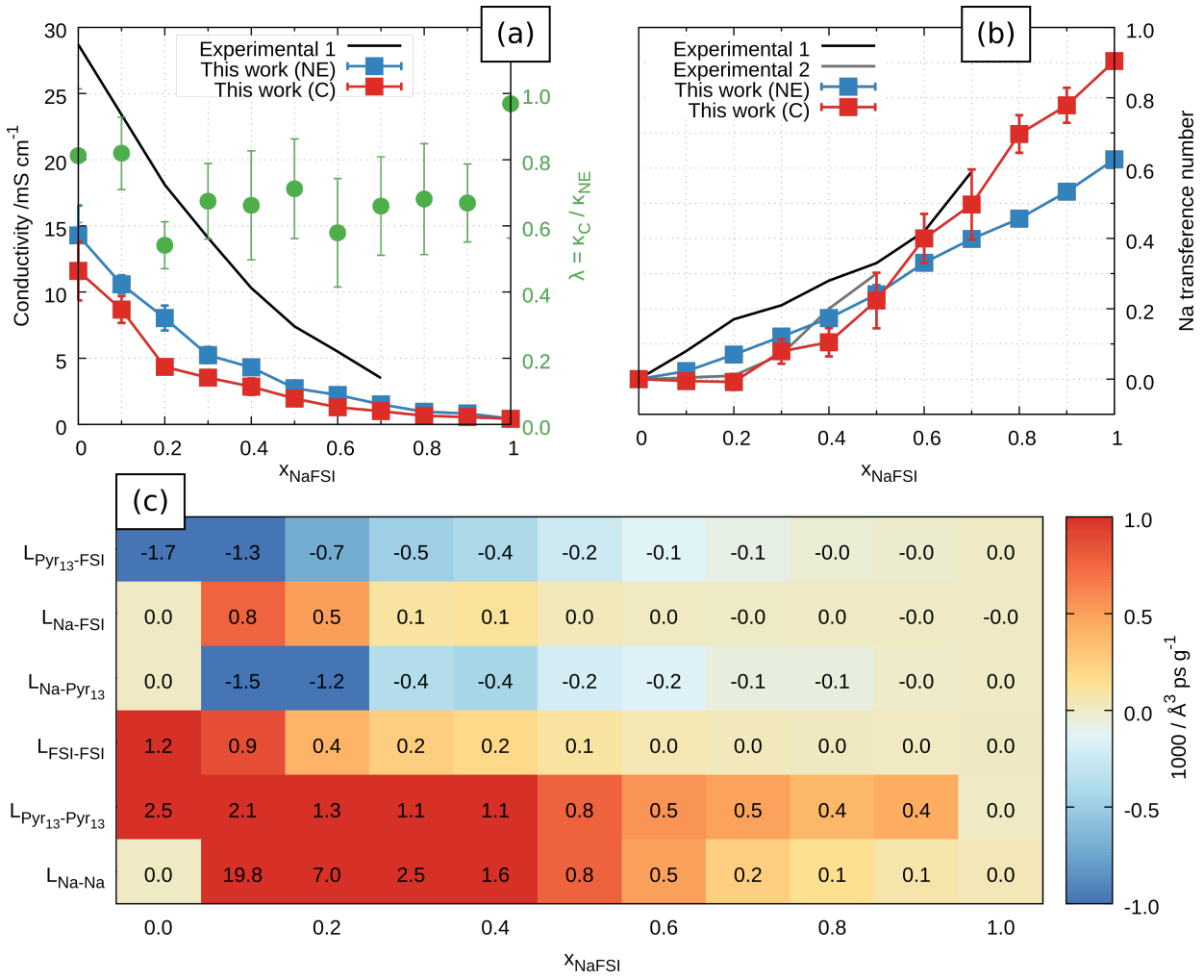

Figure 5: Summary of the transport properties for Na^+FSI^- in $Pyr_{13}{}^+FSI^-$. Plot (a) shows the conductivity values as a function of the x_{NaFSI} from experiment and our computation on the left y axes, and the ratio $\lambda = \kappa_C/\kappa_{NE}$ on the right y axes. Plot (b) shows the experimental and molecular dynamics values for t^+_{Na}. The color code is the same for both (a) and (b), i.e., black line from experiment in,[22] gray line from experiment in,[12] blue squares/line our work using the Nernst-Einstein approach, and red squares/line our work using the fully correlated approach. Plot (c) summarizes the values of all the entries of the L_{ab} matrix at all x_{NaFSI}.

ity. On the other hand, an underestimation in the absolute values of transport properties from MD simulations can be generally expected,[40,41,47–50] and further charge reduction would worsen the agreement with experiment for other bulk properties such as density and structure. A more substantial charge rescaling would require altering other parameters of the force-field in order to match density and structure of the system. As we focus on the role of ionic correlation, both in terms of relative transport properties and structure, the ad-hoc

development of a force-field to exactly reproduce the absolute values for the transport properties of Na^+FSI^- in $Pyr_{13}{}^+FSI^-$ is deemed beyond the scope of this work, and therefore a charge rescaling of 75 % of the OPLS force-field from Schrodinger Inc.[30] is considered a reasonable compromise.

The total conductivity, as computed with both the uncorrelated and correlated methods, steadily decreases as a function of x_{NaFSI}, consistent with experimental results.[22,24] Between $x_{NaFSI} = 0.1$ and $x_{NaFSI} = 0.7$, the Nernst-Einstein conductivity drops from 10.6 mS cm^{-1} to 1.5 mS cm^{-1} (86 % drop), the conductivity from the correlated analysis is reduced from 8.7 mS cm^{-1} to 1.0 mS cm^{-1} (88 % drop), and the experimental[22] decreases from 23.4 mS cm^{-1} to 3.5 mS cm^{-1} (85 % drop). The uncertainty of the computed conductivity values for the four structures with equal x_{NaFSI} is generally small, indicating a weak dependence of the conductivity on the initial structure. This observation gives us confidence that the adopted number of independently-generated structures is sufficient, and the results statistically robust. The ratio between the conductivity values from the Nernst-Einstein and the correlated approach, λ, is between 0.6 and 0.8, with the only exception being $x_{NaFSI} = 1.0$, which correspond to a pure Na^+FSI^- salt system and has $\lambda \approx 1$. The meaning of $\lambda < 1$ is that the intra- and inter-species correlations have an overall negative effect on the total conductivity, lowering its value as compared to the case where these correlations are ignored. Furthermore, $\lambda \neq 1$ indicates that results obtained using the uncorrelated Nernst-Einstein approach are not capturing the full transport features of the system.

Figure 5(b) shows t^+_{Na} as a function of x_{NaFSI} from two experimental works, and our study. Both experimental works[12,22] (black and gray lines) adopt the Bruce-Vincent method for measuring the t^+_{Na}.[26,27] The authors in Ref.[12] highlight how their t^+_{Na} findings agree with those of Ref.[22] for $x_{NaFSI} = 0.4$ or greater. However, they do not address the differences between the two measurements in the range $x_{NaFSI} = 0.1$ to $x_{NaFSI} = 0.3$, which might be

caused by dissimilarities in the experimental setups. Given the apparently identical setup of the two set of measurements, we believe it is likely that these results differ due to experimental uncertainties. Interestingly, the steady increase in t^{+}_{Na} found in Ref.[22] (black line) is reproduced by our Nernst-Einstein estimation using Eq. 4, while the practically-zero sodium transference number up to approximately $x_{NaFSI} = 0.2$ observed in Ref.[12] (gray line) is very well captured by our calculations using the fully-correlated approach, Eq. 8. It should be noted that experimental measurements using the rigorous approach based on concentrated-solution theory as developed by Newman and coworkers[25,51] should provide more reliable results than the widely-used analysis by Bruce and Vincent,[26,27] which assumes that the electrolyte exhibits ideal solution behavior.

Similarly, in order to use MD-based approaches to compute conductivity and transference number it is important to take into account the full amount of correlation, which is systematically overlooked in the literature even in the case of such highly-correlated systems. For instance, recent experimental findings report negative transference numbers for both polymer based[15] and different salt/ionic liquid[16] electrolytes. A negative transference number can be obtained when vehicular transport mechanism for the cation of interest prevails, the "vehicle" being a cluster with overall negative charge, containing a higher number of anions than cations.[15,16,40] Comparing the transference number as obtained from Eq. 4 (uncorrelated motion of the ions) and Eq. 8 (full accounting of the intra- and inter-species correlation), only the latter can yield negative values, and thus uncover and help explain the physics of the system.

In fact, specifically for the $Na^{+}FSI^{-}$ in $Pyr_{13}{}^{+}FSI^{-}$ system, we do report a negative transference number of $t_C^{Na^+} = -0.006$ and $t_C^{Na^+} = -0.008$ for $x_{NaFSI} = 0.1$ and $x_{NaFSI} = 0.2$, respectively. The near-zero transference number observed in experiments (gray line from Ref.[12]) for x_{NaFSI} up to $x_{NaFSI} = 0.2$ was conjectured to stem from either neutral or nega-

tively charged Na^+FSI^- aggregates of low mobility[12] that do not contribute or contribute negatively to the Na^+ conductivity. The presence of neutral clusters is highly unlikely at these low x_{NaFSI}, as FSI^- has four oxygen atoms (and it is the only species with oxygen atoms), and, consistent with the literature, we showed that Na^+ is systematically coordinated by 5/6 oxygen atoms (and the distribution of coordination is peaked the most for these low x_{NaFSI}). As a result, the smallest Na^+FSI^- aggregate containing only one Na^+ has to include *at least* two FSI^- anions to satisfy the Na^+ coordination. Ignoring the possibility of neutral clusters and acknowledging that the coordination is very much peaked at 5/6 oxygen atoms, the overwhelming presence of negatively charged clusters would result in an important contribution of the vehicular mechanism to the total transport. This would explain a negative t^+_{Na}, which experimentally could be hidden by the intrinsic assumptions of the Bruce-Vincent analysis, which is only valid for ideal solutions and cannot measure negative transference numbers.[26,27]

The appearance of negative transference number at low x_{NaFSI} is unexpected. In other reported cases of negative transference number, it occurs at high concentration. For instance, for aqueous ZnCl a negative transference number has been reported for salt molar concentrations exceeding 2 M.[52] For LiTFSI in PEO electrolyte system a negative lithium transference number has been measured[15] for salt concentrations above $r = 0.12$. At low salt concentration Li atoms are almost entirely coordinated by the oxygen atoms from the PEO backbone, and asymmetrical clustering between Li cations and TFSI anions was shown to become increasingly important at high LiTFSI salt concentration.[40] We anticipate the opposite being true for the Na^+FSI^--$Pyr_{13}{}^+FSI^-$ ionic liquid system. Due to the ionic nature of the system, based on electrostatic considerations, aggregates between Na^+ cations and FSI^- anions are expected to be present even at small x_{NaFSI}. On the other hand, at higher x_{NaFSI} bigger Na^+FSI^- clusters should appear, consequently the fraction Na^+ cations to coordinating FSI^- anions increases, up to the limit of $x_{NaFSI} = 1.0$, where the system is expected to be in a single neutral cluster spanning the entire system. As t^+_{Na} goes from neg-

ative to positive and steadily increasing between $x_{NaFSI} = 0.2$ and $x_{NaFSI} = 0.3$, Figure 5(b), we anticipate a profound difference in the cluster population between these two x_{NaFSI}.

Lastly, Figure 5(c) summarizes the entries of the L_{ab} matrix for all x_{NaFSI}. A negative L_{ab} has the physical meaning that species a moves on average opposite to species b. The bottom three rows of Figure 5(c) correspond to the intra-species correlated self-diffusion ($a = b$), and are positive by definition. As x_{NaFSI} increases, the magnitude of L_{ab} decreases as observed in the self-diffusivity values.[22,24] More interesting are the top three rows of Figure 5(c), which correspond to the cases $a \neq b$. In the first column, corresponding to $x_{NaFSI} = 0.0$, $L_{Na^+FSI^-}$ and $L_{Na^+Pyr_{13}^+}$ are zero as no $Na^+$is present in the system, while $L_{Pyr_{13}^+FSI^-}$ is negative. In our MD simulations, the total center of mass of the system is at rest by conservation of total momentum. As a consequence, if the center of mass of one species moves in one direction, the other has to compensate by moving in the opposite direction. For $x_{NaFSI} = 0.1$ and $x_{NaFSI} = 0.4$ (but predominantly up to $x_{NaFSI} = 0.2$), Na^+ and FSI^- have a non-zero, positive correlation, reinforcing the conjecture that they aggregate in clusters, which then diffuse together. Consistent with this picture is the negative sign characterizing $L_{Na^+Pyr_{13}^+}$ and $L_{Pyr_{13}^+FSI^-}$.

Na^+FSI^- Clustering

The presence of asymmetric Na^+FSI^- aggregates has been extensively used to rationalize our findings. Thanks to the molecular resolution of our simulations, now we can analyze the cluster population and thereby cementing the understanding of the physics of this system. We analyze clusters of Na^+ cations and FSI^- anions by looking at their spatial correlation during the simulation, i.e., agglomerates where anions and cations are located nearby. Here we use the same data as in Figure 4. At every snapshot, clusters (or, equivalently, agglomerates) are identified following a variant of the single-linkage clustering algorithm previously used for such analysis:[40] iteratively, Na^+ and FSI^- are grouped based on a threshold distance of

3.65 Å between Na^+ and oxygen atoms from FSI^-. The 3.65 Å distance criteria correspond to the location of the first minimum of the Na^+-O radial distribution function, Figure 3. With $(C_i, A_j)^{i-j}_{j/i}$ we denote an agglomerate comprising i **C**ations (Na^+), j **A**nions (FSI^-), charge $i-j$, and j/i number of anions coordinating a cation on average. At every snapshot and for all four structures at every x_{NaFSI}, the composition and number of appearances of every cluster is saved. The final reported cluster frequency is the ratio between the number of cluster appearances and the total number of appearances of all clusters.

Figure 6 presents a graphical summary of our findings. Plot (a) to (e) show the frequency of appearance of all the clusters for selected x_{NaFSI}: (a): $x_{NaFSI} = 0.1$, (b): $x_{NaFSI} = 0.2$, (c): $x_{NaFSI} = 0.3$, (d): $x_{NaFSI} = 0.4$, and (e): $x_{NaFSI} = 1.0$. The numbers i of Na^+ and j of FSI^- participating to a given $(C_i, A_j)^{i-j}_{j/i}$ cluster are reported on the x and y axis, respectively. The vertical black line indicates the total number of Na^+ present in the structures at a given x_{NaFSI}, and therefore it constitutes an upper limit to the Na^+ in the clusters. The oblique black line corresponds to $i = j$, i.e., same number of cations and anions.

First we observe that *all* clusters lie above the $i = j$ line, in other words, FSI^- molecules systematically outnumber Na^+ cations in clusters, confirming our earlier hypothesis on the presence of asymmetrical clusters. The only exception is $x_{NaFSI} = 1.0$ where 100 % of the cluster population has $i = j$ (and there is only one single cluster extending in all the volume, Figure 6(h)), however, this can be trivially explained by the fact that it corresponds to a pure salt structure. It is worth reiterating that the overall simulation is charge neutral, consequently, the other cation in the structure, Pyr_{13}^+, balances the overall negative Na^+FSI^- agglomerates. At low x_{NaFSI}, the most likely agglomerates including one Na^+ is $(C_1, A_5)^{-4}_{5.0}$, where five FSI^- molecules provide the 5/6 oxygen atoms coordination Figure 6(f), and not a single instance of neutral $(C_1, A_1)^0_{1.0}$ (or higher order neutral cluster) is found. For larger clusters comprising more than one Na^+ (for instance two as in Figure 6(g)), a fraction

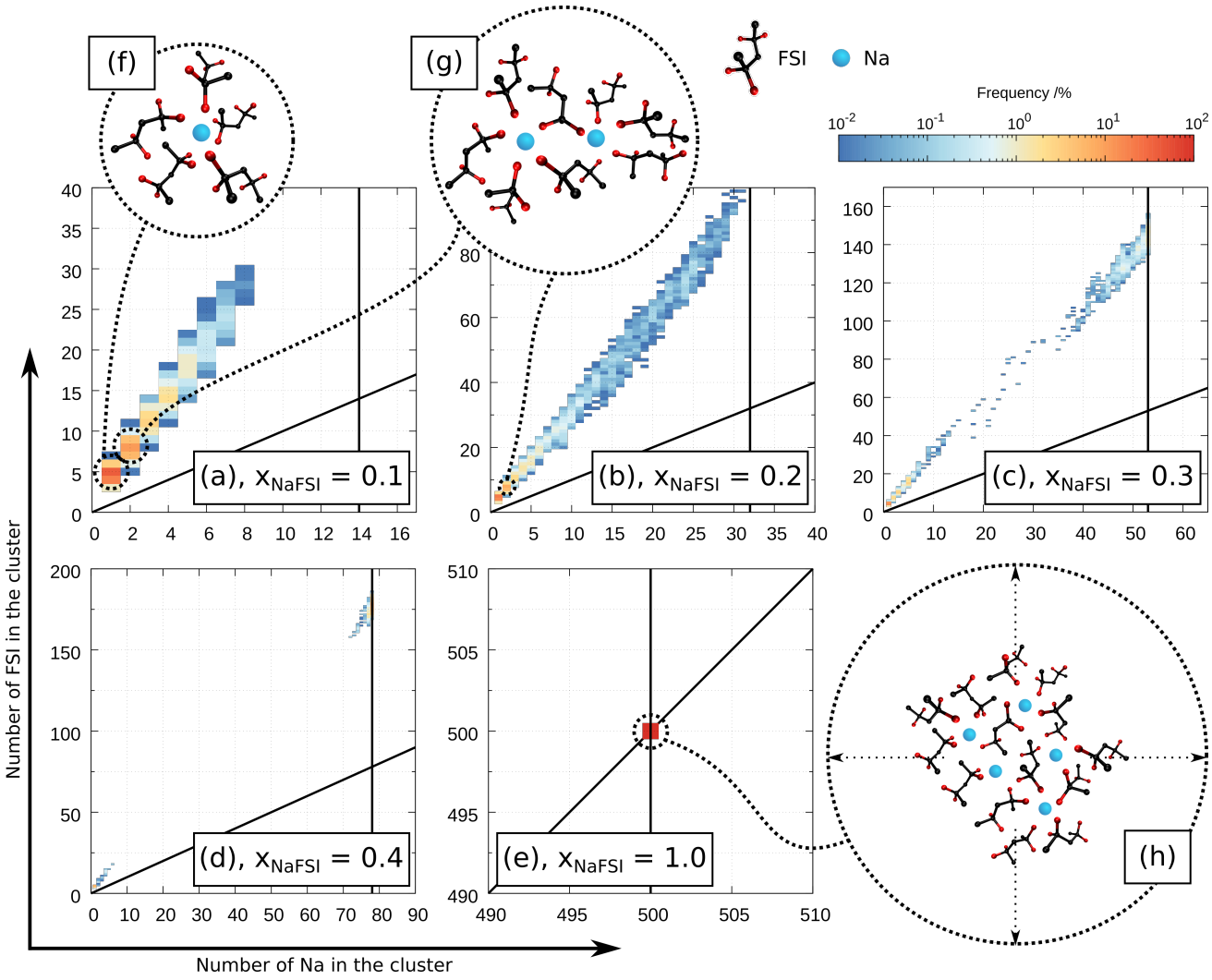

Figure 6: Summary of the clustering analysis performed on the Na^+FSI^- in $Pyr_{13}{}^+FSI^-$ system. Plots (a): $x_{NaFSI} = 0.1$, (b): $x_{NaFSI} = 0.2$, (c): $x_{NaFSI} = 0.3$, (d): $x_{NaFSI} = 0.4$, and (e): $x_{NaFSI} = 1.0$. On the x and y axes there is the number of **C**ations (Na^+) and **A**nions (FSI^-) in a given cluster. The color code indicates the frequency of a given agglomerate. In all plots, the vertical black line shows the maximum number of Na^+ in the system, Section 1 of the Supplementary Information, and the oblique line $i = j$. (f), (g), and (h) are sketches of different aggregates: (f) and (g) most likely clusters involving one and two Na^+, respectively, (h) a cluster extending over the entire system.

of the FSI^- molecules is shared among more than one Na^+ cation, consequently lowering the the average number of FSI^- molecules required to satisfy the sodium coordination. At $x_{NaFSI} = 0.2$, there appear instances of bigger clusters almost including all Na^+ in the system, albeit very rare, and smaller clusters such as $(C_1, A_5)^{-4}_{5.0}$, $(C_1, A_4)^{-3}_{4.0}$, and $(C_2, A_8)^{-6}_{4.0}$ still dominates the overall population of agglomerates. At $x_{NaFSI} = 0.3$ we observe an interesting

change in behavior: the cluster population is polarized in either small clusters *or* clusters nearly including all Na^+, and essentially nothing in between. This effect becomes more and more prominent the higher the x_{NaFSI} after $x_{NaFSI} = 0.4$, and at the same time the "single cluster" extreme dominates the cluster population. Interestingly, $x_{NaFSI} = 0.3$ coincides with t^+_{Na} becoming positive, and steadily increasing for each subsequent x_{NaFSI}. The single cluster extreme corresponds to a percolated Na^+FSI^- salt region, in which Na^+ cations are more mobile than the FSI^- molecules, essentially moving towards a single diffusing ion situation. Thus, the more dominant is this configuration, the higher is t^+_{Na}. This explains the steadily increasing t^+_{Na} once the threshold of $x_{NaFSI} = 0.3$ is overcome.

To more precisely quantify the relative importance of each cluster at every x_{NaFSI}, in Section 8 of the Supplementary Information we report the top four most frequent clusters, along with their percentage frequency. Here the main results are briefly discussed. At $x_{NaFSI} = 0.1$, the agglomerates containing at most two Na^+ have a cumulative frequency of over 81 %, and 54 % for $x_{NaFSI} = 0.2$, therefore accounting for the majority of clusters. At these x_{NaFSI}, the system is organized in small negative Na^+FSI^- clusters floating in a sea of $Pyr_{13}{}^+$, which act as charge-balancing cation. At $x_{NaFSI} = 0.3$, despite the most frequent agglomerates are still containing a few sodium cations, the fraction of small clusters containing at most two Na^+ drops to 31 %, and to 12 % for $x_{NaFSI} = 0.4$. This confirms the visual clues from Figure 6(c), where the cluster population is essentially divided in either small, unconnected clusters or a single cluster. t^+_{Na} becomes positive at $x_{NaFSI} = 0.3$, Figure 5(b), in good agreement with the lower relative importance of small cluster as opposed to big clusters. From $x_{NaFSI} = 0.4$ onward, the distribution of agglomerates becomes more and more polarized towards bigger clusters, and the most frequent as well as the one accounting for the majority include all the Na^+ in the system. Furthermore, the expected trend as a function of x_{NaFSI} of fewer FSI^- molecules on average coordinating a given Na^+ is clearly observed. The bigger the cluster is, the higher the fraction of FSI^- anions shared

among multiple Na^+ cations (Figure 6(f),(g)). This can also be used to explain the broader distribution in sodium coordination observed in Figure 4(b). Intuitively, when the system contains many more FSI^- anions than Na^+ cations, we showed that they organize in small clusters, which have to satisfy fewer Na^+ coordination and hence a more peaked distribution of coordination is to be expected. On the other hand, in the limit of $x_{NaFSI} = 1.0$ and, therefore, one FSI^- anion per Na^+ cation on average, the structure has less configurational freedom and a broader spectrum of coordination can be observed.

Conclusions

In this work we used a combination of molecular dynamics simulations with concentrated solution theory to highlight the importance of ion-ion correlation on the transport properties of ionic liquids for battery electrolytes. A fully correlated approach is systematically overlooked in the literature in favor the dilute-limit approach, which ignores correlations and therefore cannot capture the full complexity of the system.

In the case of the promising Na^+-$Pyr_{13}{}^+$-FSI^- electrolyte system we demonstrate that the inclusion of full correlation in the analysis yields qualitatively different predictions from approximate uncorrelated methods based on Nernst-Einstein equations. In particular, a surprisingly low and even negative transference number is observed for x_{NaFSI} lower than $x_{NaFSI} = 0.2$. This result also questions the applicability, even at moderate concentrations, of the popular Bruce-Vincent measurement technique which is based on ideal solution theory and cannot predict negative transference number. A negative transference number indicates that the cations move in the "wrong" direction, opposite to the direction expected from the electrical potential gradient, limiting the charge-discharge rate capability of the battery. At higher concentrations the transference number is found to become positive and to steadily increase to values closely matching the experimentally observed trend. Our simulations confirms the hypothesis that these behaviors are caused by the formation of asymmetric ion

clusters.

We systematically characterize the nature of such agglomerates at different x_{NaFSI}. The most prominent observation is a sharp difference in the cluster size distribution between $x_{NaFSI} = 0.2$ and $x_{NaFSI} = 0.3$, which correlates with the transition from negative to positive of t^{+}_{Na}. At low x_{NaFSI} the majority of clusters are negatively charged, so that Na^{+} is effectively drifting with the FSI^{-} molecules constituting its coordination, contributing negatively to the transference number. At sodium molar fractions larger than $x_{NaFSI} = 0.3$, a single large cluster accounting for all Na^{+} in the system becomes prominent, indicating the transition towards a solid-state system rather than an ionic liquid one.

In summary, we emphasize the general importance of a rigorous approach based on concentrated non-ideal solution theory for both experimental and theoretical studies, which should be adopted more broadly for investigating similar systems where strong interactions lead to non-trivial transport phenomena resulting from the formation of asymmetric cation-anion clusters.

Conflict of Interests

There authors declare no competing financial interests.

Supporting Information Available

Supporting Information: Specific number of atoms/molecules at every x_{NaFSI}, details of the equilibration procedure, example plots for MSD and PCF over time, density values at different temperatures for different charge rescaling factors, density values at different temperature for all the investigated x_{NaFSI}, details on the RDF calculations, coordination histograms, clustering table. This material is available free of charge via the Internet at `http://pubs.acs.org/`.

References

(1) Tarascon, J.-M. *Nature chemistry* **2010**, *2*, 510.

(2) Slater, M. D.; Kim, D.; Lee, E.; Johnson, C. S. *Advanced Functional Materials* **2013**, *23*, 947–958.

(3) Ponrouch, A.; Monti, D.; Boschin, A.; Steen, B.; Johansson, P.; Palacin, M. *Journal of Materials Chemistry A* **2015**, *3*, 22–42.

(4) Burns, J.; Kassam, A.; Sinha, N.; Downie, L.; Solnickova, L.; Way, B.; Dahn, J. *Journal of The Electrochemical Society* **2013**, *160*, A1451–A1456.

(5) Kubota, K.; Komaba, S. *Journal of The Electrochemical Society* **2015**, *162*, A2538–A2550.

(6) Yabuuchi, N.; Kubota, K.; Dahbi, M.; Komaba, S. *Chemical reviews* **2014**, *114*, 11636–11682.

(7) Palomares, V.; Serras, P.; Villaluenga, I.; Hueso, K. B.; Carretero-González, J.; Rojo, T. *Energy & Environmental Science* **2012**, *5*, 5884–5901.

(8) Frenkel, D.; Smit, B. *Understanding molecular simulation: from algorithms to applications*; Elsevier, 2001; Vol. 1.

(9) Allen, M. P.; Tildesley, D. J. *Computer simulation of liquids*; Oxford university press, 2017.

(10) Payne, V.; Forsyth, M.; Ratner, M.; Shriver, D.; De Leeuw, S. *The Journal of chemical physics* **1994**, *100*, 5201–5210.

(11) Chen, F.; Howlett, P.; Forsyth, M. *The Journal of Physical Chemistry C* **2017**, *122*, 105–114.

(12) Forsyth, M.; Yoon, H.; Chen, F.; Zhu, H.; MacFarlane, D. R.; Armand, M.; Howlett, P. C. *The Journal of Physical Chemistry C* **2016**, *120*, 4276–4286.

(13) Lourenço, T. C.; Zhang, Y.; Costa, L. T.; Maginn, E. J. *The Journal of Chemical Physics* **2018**, *148*, 193834.

(14) Vicent-Luna, J. M.; Azaceta, E.; Hamad, S.; Ortiz-Roldán, J. M.; Tena-Zaera, R.; Calero, S.; Anta, J. A. *ChemPhysChem* **2018**,

(15) Pesko, D. M.; Timachova, K.; Bhattacharya, R.; Smith, M. C.; Villaluenga, I.; Newman, J.; Balsara, N. P. *Journal of The Electrochemical Society* **2017**, *164*, E3569–E3575.

(16) Gouverneur, M.; Schmidt, F.; Schönhoff, M. *Physical Chemistry Chemical Physics* **2018**, *20*, 7470–7478.

(17) Armand, M.; Endres, F.; MacFarlane, D. R.; Ohno, H.; Scrosati, B. *Materials For Sustainable Energy: A Collection of Peer-Reviewed Research and Review Articles from Nature Publishing Group*; World Scientific, 2011; pp 129–137.

(18) Olivier-Bourbigou, H.; Magna, L. *Journal of Molecular Catalysis A: Chemical* **2002**, *182*, 419–437.

(19) Balducci, A. *Topics in Current Chemistry* **2017**, *375*, 20.

(20) Lewandowski, A.; Świderska-Mocek, A. *Journal of Power Sources* **2009**, *194*, 601–609.

(21) Watanabe, M.; Thomas, M. L.; Zhang, S.; Ueno, K.; Yasuda, T.; Dokko, K. *Chemical reviews* **2017**, *117*, 7190–7239.

(22) Matsumoto, K.; Okamoto, Y.; Nohira, T.; Hagiwara, R. *The Journal of Physical Chemistry C* **2015**, *119*, 7648–7655.

(23) Girard, G.; Hilder, M.; Zhu, H.; Nucciarone, D.; Whitbread, K.; Zavorine, S.; Moser, M.; Forsyth, M.; MacFarlane, D.; Howlett, P. *Physical chemistry chemical physics* **2015**, *17*, 8706–8713.

(24) Ding, C.; Nohira, T.; Hagiwara, R.; Matsumoto, K.; Okamoto, Y.; Fukunaga, A.; Sakai, S.; Nitta, K.; Inazawa, S. *Journal of Power Sources* **2014**, *269*, 124–128.

(25) Balsara, N. P.; Newman, J. *Journal of The Electrochemical Society* **2015**, *162*, A2720–A2722.

(26) Evans, J.; Vincent, C. A.; Bruce, P. G. *Polymer* **1987**, *28*, 2324–2328.

(27) Bruce, P. G.; Vincent, C. A. *Journal of electroanalytical chemistry and interfacial electrochemistry* **1987**, *225*, 1–17.

(28) Fadel, E.; Faglioni, F.; Samsonidze, G.; Molinari, N.; Merinov, B. V.; WA III, G.; Grossman, J. C.; Mailoa, J. P.; Kozinsky, B. **2018**,

(29) Plimpton, S. *Journal of computational physics* **1995**, *117*, 1–19.

(30) others,, et al. *Journal of computational chemistry* **2005**, *26*, 1752–1780.

(31) Doherty, B.; Zhong, X.; Gathiaka, S.; Li, B.; Acevedo, O. *Journal of chemical theory and computation* **2017**, *13*, 6131–6145.

(32) Mogurampelly, S.; Ganesan, V. *J. Chem. Phys.* **2017**, *146*, 074902.

(33) Pal, T.; Beck, C.; Lessnich, D.; Vogel, M. *The Journal of Physical Chemistry C* **2017**, *122*, 624–634.

(34) Borodin, O. *The Journal of Physical Chemistry B* **2009**, *113*, 11463–11478.

(35) Schröder, C.; Steinhauser, O. *The Journal of chemical physics* **2010**, *133*, 154511.

(36) Hoover, W. G. *Physical review A* **1985**, *31*, 1695.

(37) Nosé, S. *The Journal of chemical physics* **1984**, *81*, 511–519.

(38) Hoover, W. G. *Physical Review A* **1986**, *34*, 2499.

(39) Molinari, N.; Khawaja, M.; Sutton, A.; Mostofi, A. *The Journal of Physical Chemistry B* **2016**, *120*, 12700–12707.

(40) Molinari, N.; Mailoa, J. P.; Kozinsky, B. *Chemistry of Materials* **2018**, *30*, 6298–6306.

(41) Borodin, O.; Smith, G. D.; Henderson, W. *The Journal of Physical Chemistry B* **2006**, *110*, 16879–16886.

(42) Wheeler, D. R.; Newman, J. *J. Phys. Chem. B* **2004**, *108*, 18353–18361.

(43) Newman, J.; Thomas-Alyea, K. E. *Electrochemical systems*; John Wiley & Sons, 2012.

(44) Chen, C.-Y.; Kiko, T.; Hosokawa, T.; Matsumoto, K.; Nohira, T.; Hagiwara, R. *Journal of Power Sources* **2016**, *332*, 51–59.

(45) Molinari, N.; Sutton, A.; Mostofi, A. *Physical Chemistry Chemical Physics* **2018**, *20*, 23085–23094.

(46) Webb, M. A.; Jung, Y.; Pesko, D. M.; Savoie, B. M.; Yamamoto, U.; Coates, G. W.; Balsara, N. P.; Wang, Z.-G.; Miller III, T. F. *ACS central science* **2015**, *1*, 198–205.

(47) Wang, J.; Hou, T. *Journal of computational chemistry* **2011**, *32*, 3505–3519.

(48) Zhou, X.; Chen, Z.; Delgado, F.; Brenner, D.; Srivastava, R. *Journal of The Electrochemical Society* **2007**, *154*, B82–B87.

(49) Meunier, M. *The Journal of chemical physics* **2005**, *123*, 134906.

(50) Khawaja, M. *Imperial College London PhD thesis repository* **2016**,

(51) Doyle, M.; Newman, J. *Journal of The Electrochemical Society* **1995**, *142*, 3465–3468.

(52) Robinson, R. A.; Stokes, R. H. *Electrolyte solutions*; Courier Corporation, 2002.